14th AIAA/CEAS Aeroacoustics Conference
(29th AIAA Aeroacoustics Con
5 - 7 May 2008, Vancouver, British Columbia Canada

AIAA 2008-2851

Investigation of flow features and acoustic radiation of a round cavity

O. Marsden*, E. Jondeau and P. Souchotte†, C. Bogey‡, C. Bailly§, D. Juvé¶
Laboratoire de Mécanique des Fluides et d'Acoustique
Ecole Centrale de Lyon & UMR CNRS 5509
36 avenue Guy de Collongue, 69134 Ecully cedex, France
http://acoustique.ec-lyon.fr

Abstract

An experimental and numerical investigation of the noise generated by a turbulent boundary layer past a cylindrical cavity is reported in this paper. This geometry is often encountered on the underneath of commercial aeroplane wings, and can contribute to airframe noise during approach phases. Turbulent flow and associated radiated noise have been experimentally characterized for various aspect ratios (cavity length-to-depth) and free-stream velocities. A direct noise computation of a specific configuration is also realized through a compressible large-eddy simulation based on an explicit filtering.

I. Introduction

Airframe noise is one of the major sources of total community-perceived aircraft noise during the approach configuration.[1] And among the different components such as landing gear, high-lift devices or tailplane, tonal noise generated by burst-disk cavities located under wings can be clearly identified even if there is no direct impact on certification levels. Noise generated by a rectangular cavity excited by a grazing flow is a well-known topic in aeroacoustics and technical reviews are available by Rockwell & Naudascher[2] or Rockwell[3] for instance. Direct noise computations have also been realized with success for two-dimensional[4] and three-dimensional configurations[5] by direct numerical simulation and large-eddy simulation respectively. Investigations of the three-dimensional flow dynamics through large-eddy simulations have also been performed[6,7] as well as the study of control techniques as a possible means of reducing noise generation. Recent syntheses of the extensive litterature on this topic can be found in Cattafesta[8] *et al.* or in Rowley and Williams.[9] Less attention has been paid however to the noise generated by a circular cylindrical cavity, except for deep cavities encountered in hydraulic side-branches, which are not the subject of this study. In the present work, self-sustained oscillations and the radiated acoustic field generated by a turbulent boundary layer past a cylindrical cavity on a flat plate are experimentally and numerically investigated.

*assistant professor, AIAA member, email: olivier.marsden@ec-lyon.fr
†research engineers
‡research scientist, AIAA member
§professor at ECL & Institut Universitaire de France, senior AIAA member
¶professor, senior AIAA member

Copyright © 2008 by the authors. Published by the American Institute of Aeronautics and Astronautics, Inc., with permission.

In the experimental part, the turbulent flow over a ten-centimeter-diameter cavity and its acoustics have been characterized for various aspect ratios and free-stream velocities. Several regimes are observed involving a feedback mechanism and a possible coupling between the self-sustained oscillations and an acoustic mode. Instabilities are shed by the upstream edge of the round cavity and are simultaneously convected and amplified by the shear layer until they impact the downstream cavity wall, thus generating noise. Pressure waves induced by the impact can create a feedback loop by synchronising the upstream shear layer oscillations, resulting in very high pressure fluctuation levels. The presence of an acoustic resonator can moreover reinforce or strongly affect these oscillations, as well as three-dimensional effects associated to the round geometry of the cavity. A particular geometry and velocity have been chosen to realize a direct noise computation using a compressible large-eddy simulation. Preliminary results are reported in the numerical part of the paper.
The present work is organized as follows. A brief description of the experimental set-up is given in Section II. A number of flow and acoustic results can be found and are discussed in Section III. Preliminary numerical results are presented in Section IV

II. Experimental Setup

Cavity noise experiments were conducted in the high-speed anechoic wind tunnel ($10 \times 8 \times 8$ m^3) of the Centre Acoustique at the Ecole Centrale de Lyon.[10] A schematic view of the installation can be seen in Figure 1. The flow exits from a rectangular nozzle with a section of 0.5 by 0.25 m, over a flat plate measuring 0.8 m in the streamwise direction by 0.6 m in the cross-flow direction. The round cavity of diameter $\mathsf{D} = 10$ cm is placed 45 cm downstream from the nozzle exit. In order to obtain a reproducible incoming tubulent boundary layer, a strip of sandpaper is placed inside the nozzle before the convergent zone, thus ensuring a complete transition to a turbulent state for all flow velocities of interest.

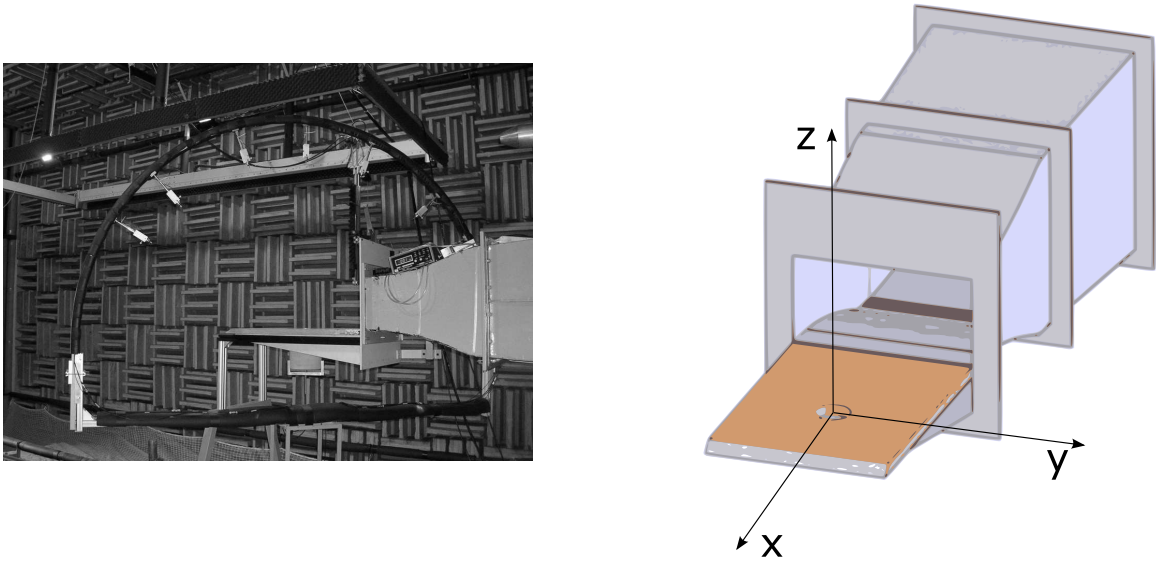

Figure 1. View of the experimental setup

The main flow and geometric parameters of the study are listed in table 1. The main part of the study deals with a cavity depth of 100 mm, but depths of 50 and 150 mm are also considered. Incoming flow velocity ranges from 50 to 110 m/s, or approximately $\mathsf{M} = 0.15$ to $\mathsf{M} = 0.34$.

The boundary layer thickness δ_{99}, also reported in table 1, varies between around 18 mm and 16 mm over this Mach number range, while the shape factor remains approximately constant at $H = \delta_\star/\delta_\theta \simeq 1.35$. Turbulence levels in the free stream are very low, and do not exceed 1% of the free-stream velocity. Maximum fluctuation levels in the boundary layer are reached at a distance of approximately 3 mm from the wall. Figure 2 shows an example of velocity profiles, both mean and rms fluctuations, measured 225 mm upstream of the cavity leading edge by LDA, for the 70 m/s case. Velocity profiles have also been measured at different values of y to ensure that the boundary layer is relatively two-dimensional upstream of the cavity. Profiles of streamwise velocity show reasonable similarity,with differences not exceeding 4 m/s throughout the boundary layer. The transversal velocity component also remains small, not exceeding 3 m/s at any of the measurement locations.

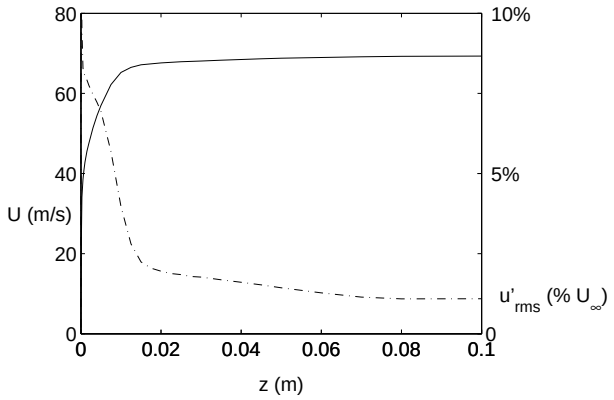

Figure 2. Case U_∞ =70 m/s. Solid black line: boundary layer profile upstream of the cavity, as a function of z. Dashed black line: profile of rms fluctuations in the boundary layer, as a function of z.

The cavity has been instrumented in order to allow the measurement of both static and fluctuating wall pressure signals. For static wall pressure measurements, 0.7 mm stainless steel tubes are flush-mounted on the cavity walls, and connected to a FURNESS© manometer with atmospheric pressure as reference. These pressure tappings are located along four vertical lines on the cylindrical wall, and along two perpendicular diameters on the cavity floor. The cavity block can be rotated with respect to the grazing flow, allowing to measure static pressure at any angular position around the cavity.

In a similar way, the cavity is fitted with a total of 20 B&K 1/4" microphones, arranged in four vertical lines comprised of four microphones each, and 4 microphones on the cavity floor. Again, the instrumented cavity can be rotated with respect to the flow in order to obtain fluctuating pressure measurements anywhere on the cavity walls. Far-field acoustic directivity measurements have also been performed, thanks to seven B&K ICP type 4935 microphones placed on a semi-circular rotating antenna centred on the cavity.

Cavity radius r	50 mm
Cavity depths h	50, 100, 150 mm
Flow velocities U_∞	50, 70, 90 m/s
Boundary layer thickness δ_{99}	17 mm

Table 1. Main parameters of the flow configuration studied.

III. Experimental results & analysis

A small number of studies[11,12] have shown that under certain conditions, the mean flow in the vicinity of a circular cavity can be asymmetrical. Hiwada *et al*[11] found that for an aspect ratio of $h/D = 0.5$, the pressure distribution on the walls of the cavity was highly asymmetrical and yet stable, while for aspect ratios both greater than 1 and lower than approximately 0.2, a symmetrical distribution was obtained. Dybenko *et al*[12] found evidence of asymmetrical configurations where a very low-frequency "flapping" was observed in the wake zone. In the present work however, the cavity depth in which we are primarily interested yields an aspect ratio of 1, and thus a symmetrical mean flow is expected. This is confirmed experimentally, as shown by the isocontour plot of the mean pressure on the cavity walls and floor, represented in Figure (3) for a freestream velocity of 70 m/s. The experimental pressure distribution obtained in this study, while less complete than that measured by Hiwada, nevertheless shows good qualitative agreement with Hiwada's data, which was obtained for a cavity diameter of $D = 65$ mm and a freestream velocity of 25 m/s.

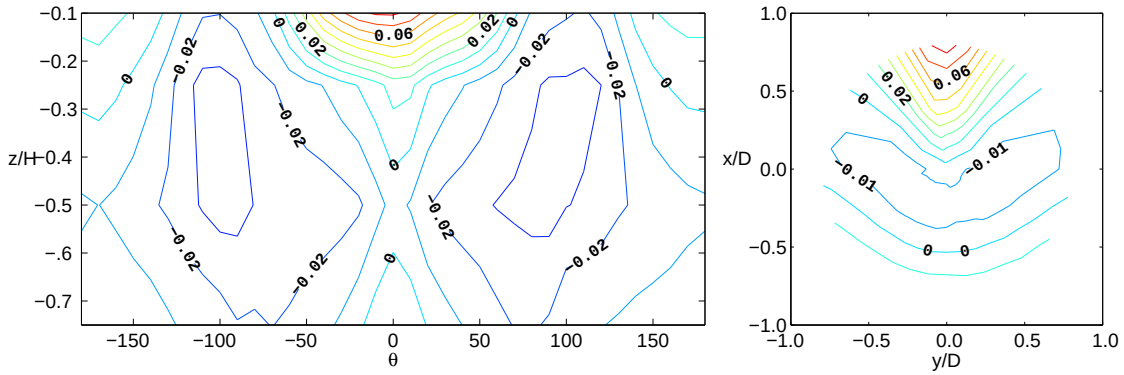

Figure 3. Experimental static pressure distribution on the cavity wall and cavity floor at 70 m/s. Contour lines between $-0.05 \times \rho U_\infty^2$ **and** $0.1 \times \rho U_\infty^2$

It is known that deep cylindrical cavities exhibit a stong acoustic resonance at their quarter-wavelength frequency. The resonant frequency of interest is given by $f_c = c_0/4(h + \delta_h)$ where $\delta_h = 0.8216 \times r$ corresponds to the acoustic correction length for an infinitely flanged open pipe.[13] For the reference cavity depth of 100 mm, this leads to a frequency of $f_c \simeq 607$ Hz. It should be noted however that the aspect ratio $2r/h$ is equal in this case to one, and in that respect the cavity should not be qualified as deep.

In the context of this study, it is interesting to note that the far-field acoustic PSD has maxima that vary strongly with flow velocity, as shown in the left-hand side of Figure 4. In fact, the three spectra in this Figure exhibit markedly different behaviours. Those measured at 50 and 90 m/s show two separate peaks which emerge from the background noise by roughly 20 dB, while that measured at 70 m/s has a single maximum at a frequency of 650 Hz, about 7% higher than f_c, which emerges from the background noise by more than 30 dB. The single peak observed at 70 m/s is noticeably sharper than the double peaks of the two other spectra. It is thus apparent that at least at 50 and 90 m/s, a depth-mode acoustic resonance of the cavity is not the main noise source. The right-hand side of Figure 4 shows the acoustic PSD at 70 m/s for three different cavity depths, as well as for the baseline flat plate case. For the cavity of 50 mm depth, there is a wide hump in the PSD at around 900-1000 Hz. This frequency range is roughly centred around the resonant frequency of $f_c = 942$ Hz for this depth, but the wide-band aspect of the hump suggests that no strong feedback mechanism between the shear layer and the acoustic emission is present. For the two deeper cavities, the peaks in the PSD also correspond to the respective resonant frequencies, but the peaks are much narrower, indicating a more resonant phenomenon in these cases.

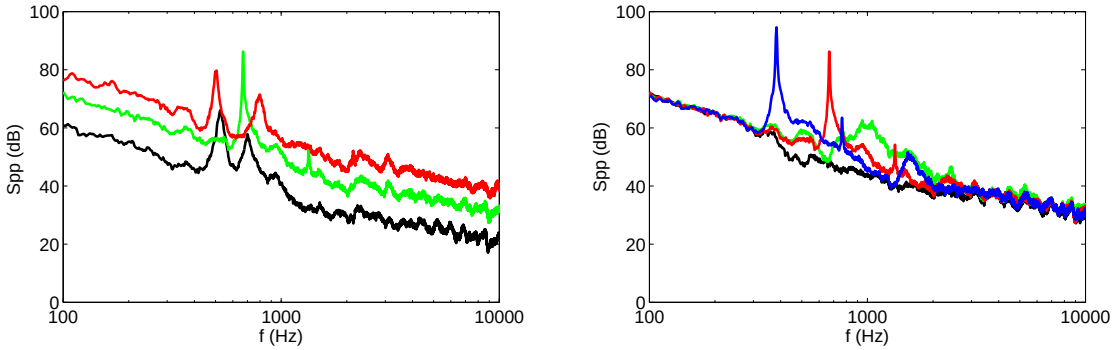

Figure 4. Left: experimental PSD (Pa^2/Hz) at 1 m above the cavity at three different flow velocities: — $U_\infty = 50$ **m/s,** — $U_\infty = 70$ **m/s,** — $U_\infty = 90$ **m/s**
Right: experimental PSD (Pa^2/Hz) at 1 m, with $U_\infty = 70$ m/s, for three cavity depths h: — $h = 0$ **mm,** — $h = 50$ **mm,** — $h = 100$ **mm,** — $h = 150$ **mm.**

The resonant nature of the configuration at 70 m/s is also illustrated by the left-hand side of Figure 5 which represents the acoustic mean squared pressure at 1 m as a function of the free-stream flow velocity. The acoustic power level can be seen to increase from 79 dB for an upstream flow velocity of 50 m/s, to 106.4 dB at 110 m/s, with a local maximum of 97.5 dB at 70 m/s. It is compared to a U_∞^6 scaling, shown as the dashed line, scaled to correspond to the experimental power level at 50 m/s. Acoustic scaling based on U_∞^6 is typical of compact dipolar noise source mechanisms, such as turbulent fluctuations close to a rigid surface. Thus a sixth power scaling would be anticipated in the absence of notable acoustic resonance in the cavity, as a result of the shear layer interaction with the downstream cavity wall. The baseline evolution of the acoustic power is well described by this scaling, but it deviates notably from the sixth power law for velocities around 70 m/s and 110 m/s. This additionnal acoustic power is assumed to be the result of resonant phenomena around these flow velocities. It should be noted that such a result does not agree with the analysis performed by Parthasarathy *et al.*,[14] according to which the acoustic power generated by a cylindrical cavity should scale with U_∞^2.
An examination of the 70m/s case gives more insight into the resonant nature of this configuration. The right-hand half of Figure 5 represents the acoustic PSD, measured at a height of 1 m above the cavity, as a function of the upstream flow velocity U_∞ and frequency for the 100 mm-deep cavity. Also represented as a solid black line is the theoretical quarter-wavelength resonance frequency of the cavity. Frequencies of the peaks in the PSD vary with velocity, suggesting that shear layer modes rather than acoustic pipe resonance are the dominating phenomenon at play. Instead, acoustic resonance appears to modulate the level of noise generated by shear layer modes, as shown by the evolution of the maximum levels. Figure 5 also explains the presence of two peaks at 50 and 90 m/s, there being two active shear layer modes of comparable level at these flow velocities.
Figure 6 also confirms this point. It represents the PSD of vertical w' velocity fluctuations at $x = 45$ mm, 5 mm upstream of the cavity downstream edge. The solid black line is measured at a height of $z = 1$ mm, while the dashed line is measured at 60 mm above the cavity, well outside the boundary layer. Two peaks are clearly visible inside the boundary layer, but cannot be seen at all in the signal measured outside the boundary layer. The peaks thus cannot be attributed solely to acoustic emission from the cavity, but indicate that the two frequencies are present inside the boundary layer. A time-frequency analysis of this signal shows no sign of mode-switching taking place between the two shear layer modes.
A different representation of acoustic level as a function of velocity is shown in Figure 7, where the SPL is now represented as a function of upstream velocity and diameter-based Strouhal number $St = fD/U_\infty$. Rossiter[15] was the first to propose a physical explanation for tonal noise generation,

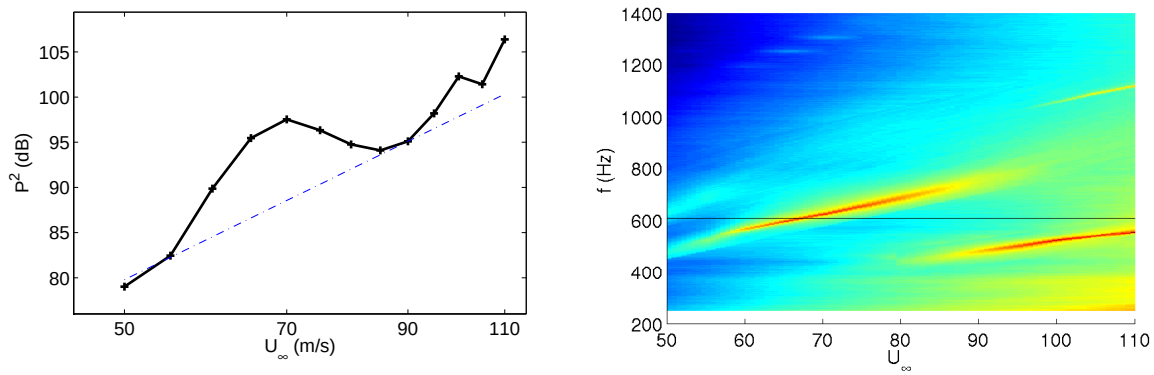

Figure 5. Left: experimental power level in dB at 1 m above the cavity, as a function of freestream velocity. -+-+- experimental data , – – – U_∞^6 scaling
Right: experimental PSD (Pa^2/Hz) at 1 m represented as a function of velocity. Colour scale between 30 and 100 dB.

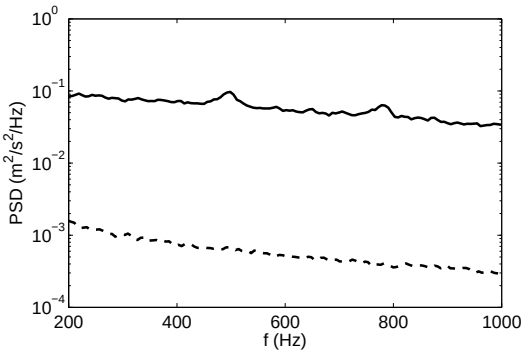

Figure 6. Experimental PSD of u and w velocity at $x = 0.045$ just upstream of the cavity downstream edge. Upstream flow velocity is 90 m/s.

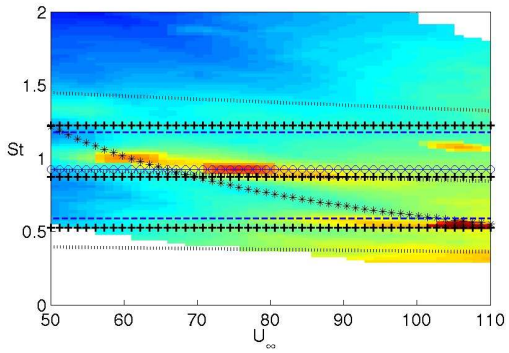

Figure 7. Experimental PSD (Pa^2/Hz) at 1 m represented as a function of velocity and diameter-based Strouhal number. Colour scale between 30 and 100 dB. Dotted black lines show the first three Rossiter modes based on the diameter. Dashed blue lines show the bounds inside which $\Im(\sigma) < 0$, and blue circles correspond to Strouhal numbers for which it is most negative.

as well as a semi-empirical relationship predicting discrete Strouhal numbers at which such tones can be observed. Rossiter reasoned that tonal amplification was due to a feedback mechanism between vorticity creation at the cavity leading edge, and the noise emitted by the same vorticity

impinging the downstream cavity wall. His relationship

$$St = \frac{fL}{U_\infty} = \frac{n - \alpha}{M + U_\infty/U_c}$$

where U_c is the average convection velocity of vortical structures in the shear layer and α is an empirical constant generally taken around 0.25, suggests that tonal amplification can take place for frequencies such that the convection time L/U_c for vortices across the cavity opening, added to the acoustic propagation time between the downstream and upstream cavity corners, L/c_∞, is a multiple of the period, where the multiple n corresponds to the average number of vortices in the shear layer. This relationship has been shown to work well for a wide variety of different rectangular cavity configurations. Its suitability for round cavities is considerably less evident, since the distance L used in the above expression is no longer constant in the cross-stream direction. It has however been plotted in dotted black lines in Figure 7 for reference, for $n = 1$, 2, and 3. It can be observed that these diameter-based Rossiter curves do not accurately represent the variation of the Strouhal number with Mach number, and in particular do not correctly approximate the slopes of the Strouhal number curves. The stars show the Strouhal number corresponding to the round cavity's quarter-wavelength resonant frequency. The maximum acoustic levels for each shear layer mode are found to lie close to the intersection between the quarter-wavelength and the shear layer Strouhal numbers. Finally, the blue dashed lines represent the lower and upper Strouhal number bounds for which the imaginary part of the Rayleigh conductivity σ of the cavity aperture is negative. These values are taken from the work by Grace *et al.*[16] For a harmonically fluctuating pressure difference at a given Strouhal number across an aperture shear layer, a negative value of the imaginary part of the conductivity will lead to the amplification of the periodic pressure difference, while a positive imaginary part will attenuate the pressure difference. Hence it is interesting to note that high acoustic levels are located mostly within these bounds, and in particular that the second shear layer mode reaches its acoustic maximum for $St = 1.9$ (blue circles), corresponding to the most negative imaginary part of the Rayleigh conductivity. The first shear layer mode reaches its maximum at a Strouhal of $St = 0.54$, which is slightly under the lower bound of the negative Rayleigh number zone. However, the mode appears to peak almost exactly at the cavity's acoustic resonance Strouhal, which might explain the high acoustic emission for this configuration. Moreover, this Strouhal number is also close to the value of 0.525, shown by Parthasarathy *et al*[14] to be one of the characteristic forcing frequencies for the cavity-flow system modeled as a simple 1-D oscillator.

In order to better characterize the behaviour of the cylindrical cavity at $U_\infty = 90$ m/s, several statistical quantities have been measured or calculated from the experimental data. Figure 8 displays the spectrogram of the pressure measured by a microphone located directly above the cavity at $z = 10H$. The two peaks are clearly visible and no intermittence is noticed between these two frequencies in the acoustic radiated field. This again suggests that mode switching is not the mechanism responsible for the presence of two peaks in the acoustic spectra. Wall-pressure-fluctuation measurements have been performed using 20 quarter-inch Bruel & Kjaer microphones. The time signals are acquired by a National Instruments PXI over 64 seconds at a sampling frequency $f_s = 12800$ Hz and power spectral densities are also directly computed by the spectral analyser using a Hanning weighting and 500 samples. Power spectral densities of the wall-pressure along the circumferential surface inside the cavity at a height of $z = -0.1H$ are reported in Figure 9. The presence of the impinging shear layer can be noticed by the high levels of wide-band noise for polar angles angles with respect to the flow direction close to $\phi = 0$, as well as the presence of the stronger peak, $f_p \simeq 500$ Hz, around the entire circumference of the cavity. The second peak $f_s \simeq 793$ Hz is decidedly less marked with a maximum amplitude roughly 10 dB lower, as in the far-field acoustic spectra, and is most strongly visible in the downstream zone of the circumferen-

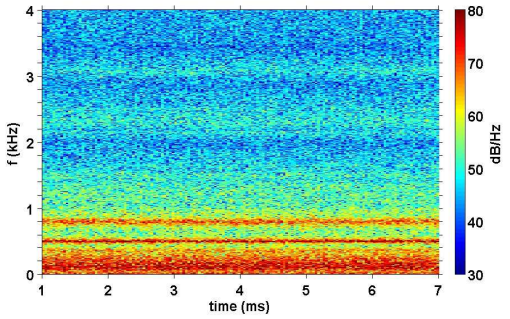

Figure 8. Spectrogram of the measured acoustic pressure at $x = y = 0$ and $z = 10H$, corresponding to an observer angle $\theta = 90$ deg., with linear frequency on the vertical axis and time on the horizontal axis.

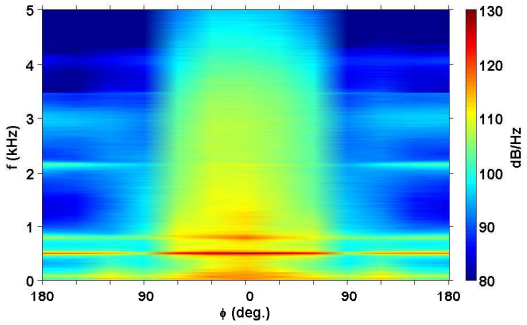

Figure 9. Fluctuating wall-pressure spectra measured at $z = -0.1H$ along the circumference inside the cavity as a function of the polar angle ϕ, where $\phi = 0$ deg. designates the downstream direction.

tial cavity wall, for polar angles between $-\pi/2 \leqslant \phi \leqslant \pi$ with respect to the flow direction. A less marked peak at approximately 2160 Hz, as well two additionnal higher-frequency peaks, can be observed in the upstream direction, but their considerably lower level means that they are masked by the wide-band turbulent-impingement-related pressure fluctuations in the downstream direction. The coherence function γ^2 between two signals u and v is defined as follows

$$\gamma^2(f) = \frac{S_{uv}\, S^{\star}_{uv}}{S_{uu}\, S_{vv}} \tag{1}$$

where S_{uv} is the cross-power spectral density function and $\star$ denotes the complex conjugate. This function is plotted in Figure 10 for the upstream and downstream fluctuating wall-pressure inside the cavity. A high coherence level is obtained for the two peaks at $z = -0.1H$, indicating an acoustic correlation for such a separation distance. A larger broadband coherence is found at $z = -0.75H$, and secondary peaks also appear.

The time delay between the upstream and downstream fluctuating wall-pressure can be estimated by computing the cross-correlation function $R_{pp}(\tau)$

$$R_{pp}(\mathbf{x}_1, \mathbf{x}_2, \tau) = \frac{\overline{p'(\mathbf{x}_1, t+\tau)\, p'(\mathbf{x}_2, t)}}{\sqrt{\overline{p'^2(\mathbf{x}_1, t)}}\, \sqrt{\overline{p'^2(\mathbf{x}_2, t)}}} \tag{2}$$

between the two signals recorded at $\mathbf{x}_1$ and $\mathbf{x}_2$. Figure 11 displays this function. The maximum correlation is found for a time delay $\Delta\tau = 0.001$ s, and can be compared to the acoustic propagation time τ_a along the distance D at an estimated velocity $\bar{c}$ lying in the interval $c - U_\infty \leqslant \bar{c} \leqslant c$, which yields $3 \times 10^{-4} \leqslant \tau_a = D/\bar{c} \leqslant 4 \times 10^{-4}$ s.

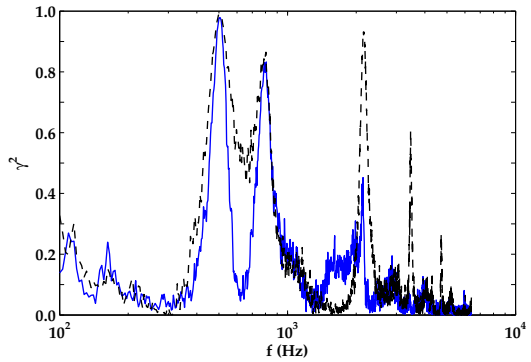

Figure 10. Magnitude squared coherence, see expression (1) between downstream, at $x = 0.5D$, and upstream, at $x = -0.5D$, fluctuating wall-pressure for two microphone depths: —— $z = -0.1H$ and – – – $z = -0.75H$.

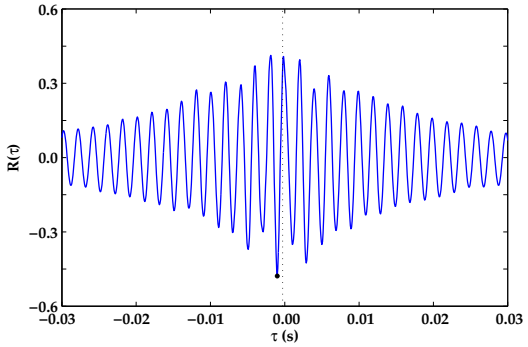

Figure 11. Normalized cross-correlation function $R_{pp}(\tau)$, defined by relation (2), between downstream and upstream wall pressure, $\mathbf{x}_1 = (0.5D, 0, -0.1H)$ and $\mathbf{x}_2 = (-0.5D, 0, -0.1H)$ respectively. The maximum correlation is marked by the symbol • and the dashed line corresponds to the estimated acoustic propagation time τ_a.

Finally, Figure 12 shows fluctuating wall pressure spectra measured on the floor of the cavity, and represented as a function of polar angle ϕ. Figure 12(a) is symmetrical by construction and included for comparison, showing the spectrum measured for $r = 0$ duplicated in the ϕ direction. The two peaks at 500 and 793 Hz are clearly visible, and both have a notably higher amplitude than around the circumference at $z = -0.1H$, previously seen in Figure 9, as expected for the closed end of a semi-open pipe configuration for frequencies close to the analytical resonant frequency of 607 Hz. Their levels remain roughly constant across the cavity floor. On Figures 12(b), (c) and (d), the impact zone of the cavity recirculation flow on the bottom surface can be seen for angles close to $\phi = 0$. The broadband nature of the spectra for these angles suggests that the impacting recirculation flow is strongly turbulent. The peak at 2160 Hz also seen in Figure 9 is more strongly visible on the cavity floor, and it exhibits a strong symmetry with respect to the flow direction, almost disappearing for $\phi = \pm\pi/2$. This peak is not a multiple of one of the two main frequencies present, nor of the cavity resonant frequency. Its origin is at present not clearly identified.
Experimental work is ongoing on this geometry. Additional validation information is being gathered, and in particular, PIV imaging techniques will be used to investigate the flow structure in and around the cavity, both for an acoustically resonant case at 70 m/s, and a configuration exhibiting two peaks, at 90 m/s.

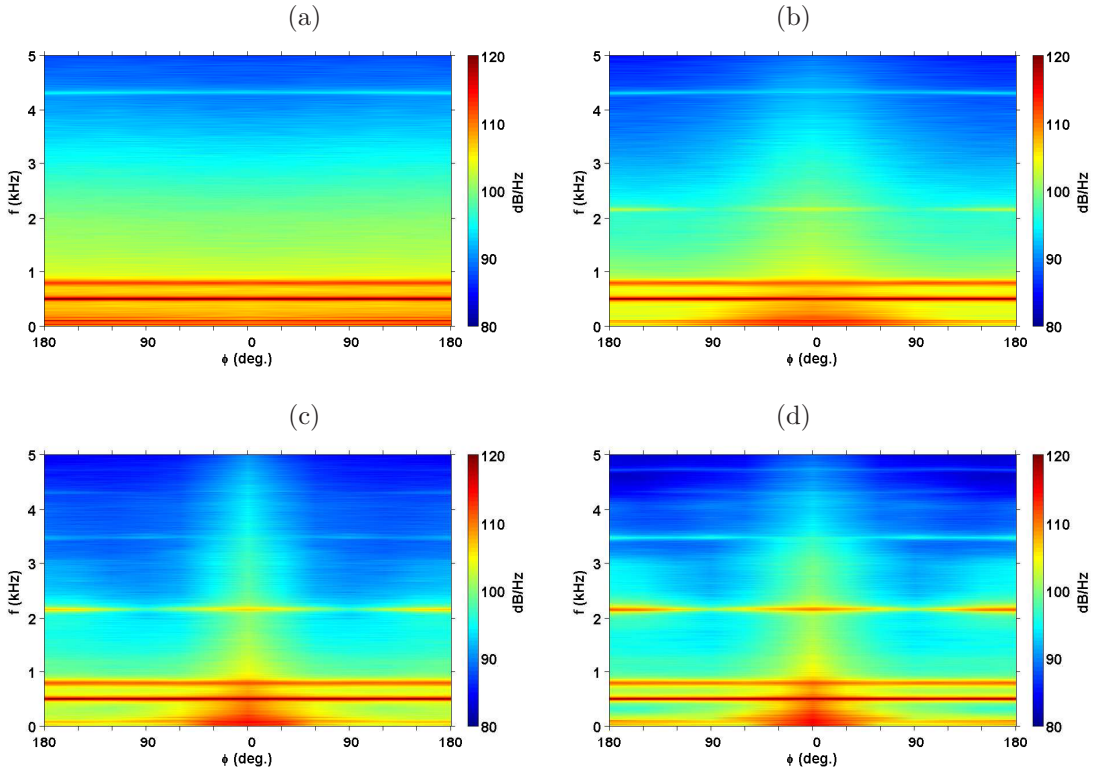

Figure 12. Fluctuating wall-pressure spectra measured over the cavity bottom as a function of the polar angle ϕ for different radial positions: (a) $r = 0$, (b) $r = D/8$, (c) $r = D/4$ and (d) $r = 3D/8$.

IV. Numerical approach

Preliminary numerical results have been obtained for the flow configuration at 90 m/s. These results are obtained from a direct noise computation of the full compressible Navier-Stokes equations. The parallel high-order finite-differences solver used in this work mixes cylindrical and Cartesian coordinates. A cylindrical approach is used to allow a body-fitted non-slip boundary condition to be imposed on the cavity wall,[17,18] while the rest of the domain is treated in a Cartesian fashion. An explicit 11-point centred finite difference scheme is used to compute derivatives inside the computational domain, and 11-point non-centred schemes are used close to boundaries. Explicit 11-point optimized 6-th order filters are used to ensure energy dissipation at the finest turbulent scales.

Details on the optimized finite differences, filters and Runge-Kutta schemes, as well as non-reflecting boundary conditions, can be found in Bogey *et al.*[19,20] High-order Lagrangian interpolation is used to provide communication between the different grids.

Preliminary results presented here were obtained over 50,000 iterations, with a time step of $\delta t = 1.18 \times 10^{-6}$ s corresponding to an acoustic CFL number of 0.72 based on the smallest grid dimension in the computational domain. The computational domain is comprised of three grids. The main Cartesian grid, corresponding to the zone above the cavity, contains $427 \times 270 \times 102$ points in the x, y and z directions respectively. This yields a spatial extent of $-0.36 < x < 0.52$, $-0.33 < y < 0.33$ and $0 < z < 0.48$. The cylindrical cavity wall is meshed by 190 points in the azimuthal direction, 25 points in the radial direction and 85 points in the vertical direction, while the cavity's Cartesian grid contains $60 \times 60 \times 85$ points in the x, y and z directions respectively.

For reasons of computational cost, the velocity field prescribed in the inflow region close to the wall is stationary, but corresponds to a mean turbulent boundary layer velocity profile computed by a

Van Driest I transformation combined with Coles' law of the wake.[21] The absence of turbulent velocity fluctuations in the boundary layer upstream of the cavity leads to an artificially fast boundary layer thickening. Hence the boundary layer thickness imposed at the incoming boundary condition is chosen smaller than that observed experimentally, and adjusted empirically to approach experimental results. Future works will examine the effect of the state of the upstream boundary layer on computational results.

A snapshot of the instantaneous velocity field in Figure 14 suggests the presence on average of two vortical shear layer structures across the streamwise cavity mouth diameter. A simplistic Rossiter model based on the cavity diameter and two shear layer vortices yields a Strouhal number of around 1.1, higher than the experimentally observed Strouhal numbers of $St = fH/U_\infty = 0.89$ and $St = fH/U_\infty = 0.56$. It is interesting to note that the experimental Strouhal number found here is quite similar to that those measured by Parthasarathy *et al*[14] on round cavities with similar diameter-to-depth ratios, since they observed a Stouhal number around $St = 0.525$.

Figure 13 shows an instantaneous view of the pressure fluctuations around the cavity in the streamwise plane of symmetry. Strong acoustic radiation is observed to be emitted from the cavity, and intense pressure fluctuations are also visible inside the cavity.

Quantitative acoustic results are estimated at a point $(x, z) = (0, 0.3)$ located 30 cm directly above the centre of the cavity. Figure 15 shows the PSD computed at this point. When the results are scaled to a distance of 1 m to be compared to experimental data, an SPL of 100.5 dB is obtained, to be compared to the 97.1 dB measured experimentally. The two acoustic peaks at around 500 and 800 Hz are observed in the computed PSD, and, at with amplitudes of 73 and 71 dB when scaled to 1 m, have comparable amplitudes to the experimental peaks of amplitude 79 and 71 db respectively. The high-frequency content of the acoustic signal is however notably overestimated. The exact source of this overestimation is not yet clear, but is probably due at least in part to the lack of grid resolution in the turbulent boundary layer. Indeed, on Figure 13 a few pressure waves can be seen propagating away from the boundary layer downstream of the cavity. Future computations will investigate this issue.

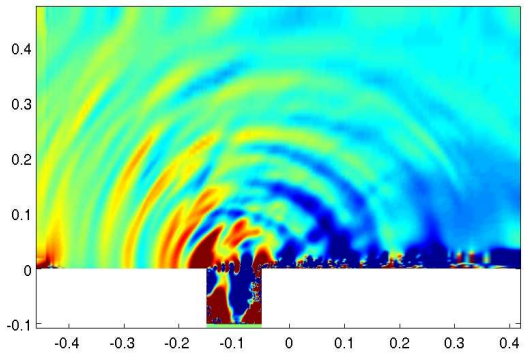

Figure 13. Computational snapshot of a streamwize cut of the fluctuating pressure field over the cavity. Colour scale between -20 and 20 Pa. Upstream flow velocity is 90 m/s.

V. Concluding remarks

Acoustic radiation by a circular cylindrical 10 mm-diameter cavity under grazing flow has been studied experimentally and numerically. Three different cavity depths of 50, 100 and 150 mm have been studied, at flow velocities between 50 and 110 m/s. For the 100 mm deep cavity, far-field

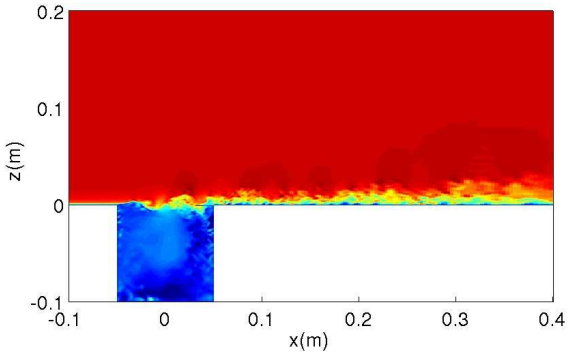

Figure 14. Computational snapshot of a streamwize cut of the velocity field over the cavity. Upstream flow velocity is 90 m/s. Colour scale between -20 and 100 m/s.

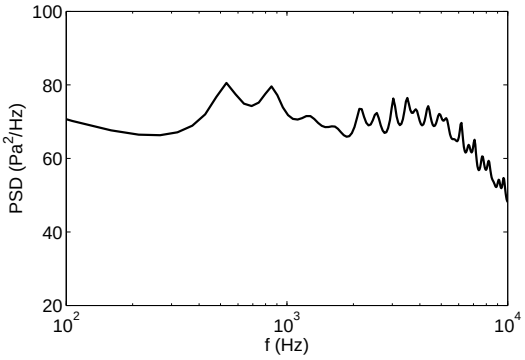

Figure 15. PSD at $(x, z) = (0, 0.3)$ obtained numerically. Upstream flow velocity is 90 m/s.

acoustic power is shown to vary roughly with the sixth power of the upstream flow velocity. Preliminary computations have been conducted for the 100 mm cavity at 90 m/s. Numerical results show reasonable agreement with experimental data, and in particular capture the two separate peaks in the acoustic PSD. Experimental data shown here, together with PIV data to be obtained shortly, will be published in a database providing detailed information for validating CFD and aeroacoustic simulation codes.

Acknowledgment

This research project is supported by the *Fondation de Recherche pour l'Aéronautique & l'Espace (FRAE)* under contract reference AFB AEROCAV, and in collaboration with following french laboratories: ONERA, SINUMEF, IUSTI and INRIA.

References

[1]Hubert, J., "Jet noise assessment and sensitivity at aircraft level," *AIAA Paper 2007-3728*, 2007, pp. 1–11.

[2]Rockwell, D. and Naudascher, E., "Review - Self-sustaining oscillations of flow past cavities," *ASME Journal of Fluids Engineering*, Vol. 100, 1978, pp. 152–165.

[3]Rockwell, D., "Oscillations of impinging shear layers," *AIAA Journal*, Vol. 21, No. 5, 1983, pp. 645–664.

[4]Rowley, C., Colonius, T., and Basu, A., "On self-sustained oscillations in two-dimensional compressible flow over rectangular cavities," *Journal of Fluid Mechanics*, Vol. 455, 2002, pp. 315–346.

[5]Gloerfelt, X., Boegy, C., and Bailly, C., "Numerical evidence of mode switching in the flow-induced oscillations by a cavity," *International Journal of Aerocoustics*, Vol. 2, No. 2, 2003, pp. 193–217.

[6]Rizzetta, D. P. and Visbal, M. R., "Large-Eddy Simulation of supersonic cavity flowfields including flow control," *AIAA Journal*, Vol. 41, No. 8, 2003, pp. 1452–1462.

[7]Larchevêque, L., S. P. L. T.-H. and Comte, P., "Large-eddy simulation of a compressible flow in a three-dimensional open cavity at high Reynolds number," *Journal of Fluid Mechanics*, Vol. 516, 2004, pp. 265–301.

[8]Cattafesta, L., Williams, D., Rowley, C., and Alvi, F., "Review of active control of flow-induced cavity resonance," *33rd AIAA Fluid Dynamics Conference*, Orlando, FL, June 2003.

[9]Rowley, C. and Williams, D., "Dynamics and control of high-Reynolds-Number flow over open cavities," *Annu. Rev. Fluid Mech.*, Vol. 38, 2006, pp. 251–276.

[10]Sunyach, M., Brunel, B., and Comte-Bellot, G., "Performances de la soufflerie anechoique grande vitesse de l'Ecole Centrale de Lyon," *Revue d'Acoustique*, Vol. 73, 1985, pp. 316–330.

[11]Hiwada, M., Kawamura, T., Mabuchi, I., and Kumada, M., "Some characteristics of flow pattern and heat transfer pas a circular cylindrical cavity," *Bulletin of the JSME*, Vol. 26, No. 220, October 1983.

[12]Dybenko, J. and Savory, E., "An experimental investigation of turbulent boundary layer flow over surface-mounted circular cavities," *CSME Forum*, 2006.

[13]Nomura, Y., Yamamura, I., and Inawashiro, S., "On the acoustic radiation from a flanged circular pipe," *J. Phys. Soc. Jap.*, Vol. 15, No. 3, 1960.

[14]Parthasarathy, S., Cho, Y., and Back, L., "Sound generation by flow over relatively deep cylindrical cavities," *J. Acoust. Soc. Am.*, Vol. 78, No. 5, 1985, pp. 1785–1795.

[15]Rossiter, J., "Wind-tunnel experiments on the flow over rectangular cavities at subsonic and transonic speeds," Tech. Rep. 3438, *Aeronautical Research Council Reports and Memoranda*, 1964.

[16]Grace, S., Horan, K., and Howe, M., "The influence of shape on the rayleigh conductivity of a wall aperture in the presence of grazing flow," *J. Fluids Struct.*, Vol. 12, 1998, pp. 335–351.

[17]Marsden, O., Bogey, C., and Bailly, C., "Turbulent Boundary Layers Around a NACA 0012 Airfoil and Their Radiated Sound," *AIAA Paper*, , No. 2006-2503, 2006.

[18]Marsden, O., Bogey, C., and Bailly, C., "Direct Noise Computation of the Turbulent flow around a zero-incidence airfoil," *AIAA Journal*, , No. 4, 2008, pp. 874–883.

[19]Bogey, C. and Bailly, C., "A family of low dispersive and low dissipative explicit schemes for noise computations," *Journal of Computational Physics*, Vol. 194, No. 1, 2004, pp. 194–214.

[20]Berland, J., Bogey, C., Marsden, O., and Bailly, C., "High-order, low dispersive and low dissipative explicit schemes for multiple-scale and boundary problems," *Journal of Computational Physics*, Vol. 224, 2007, pp. 637–662.

[21]Coles, D., "The turbulent boundary layer in a compressible fluid," *Physics of Fluids*, Vol. 7, 1964.